Earth and Planetary Science Letters 381 (2013) 210–221

Contents lists available at ScienceDirect

Earth and Planetary Science Letters

www.elsevier.com/locate/epsl

Late Pleistocene glacial advances in the western Tibet interior

William H. Amidon [a,*], Bodo Bookhagen [b], Jean-Philippe Avouac [c], Taylor Smith [b], Dylan Rood [d]

[a] Geology Department, Middlebury College, Middlebury, VT 05753, United States
[b] Geography Department, University of California Santa Barbara, Santa Barbara, CA 93106, United States
[c] Department of Geological and Planetary Sciences, California Institute of Technology, Pasadena, CA 91125, United States
[d] Scottish Universities Environmental Research Center, Glasgow, Scotland, G12 8QQ, United Kingdom

ARTICLE INFO

Article history:
Received 28 May 2013
Received in revised form 16 August 2013
Accepted 17 August 2013
Available online xxxx
Editor: T.M. Harrison

Keywords:
cosmogenic
^{10}Be
^{21}Ne
Tibet
climate
glacier

ABSTRACT

It has long been observed that the timing of glacial advances is asynchronous across the Himalaya–Karakoram–Tibet Plateau (HKTP) but the climatic implications, if any, remain unclear. Resolving this question requires additional glacial chronologies from unique spatial and climatic regimes as well as an analysis of how glaciers within different regimes are likely to have responded to past climate changes. This study presents a ^{10}Be–^{21}Ne chronology from the Mawang Kangri range of western Tibet (~34°N, 80°E); an arid high-elevation site. We identify advances at ~123, 83, and 56 kyr, which agree reasonably well with sites in the immediate vicinity, but are asynchronous relative to sites across the entire HKTP, and relative to sites in the western HKTP. To evaluate HKTP-wide asynchroneity, we compile dated glacial chronologies and classify them by the approximate timing of their maximum recent advance. This result shows a strong spatial clustering of young (MIS 1–2) relative to older (MIS 3–5) maximum advances. Further comparison with modern precipitation, temperature, and topographic data show that the pattern of HKTP-wide asynchroneity is broadly independent of topography and can potentially be explained by local responses to changes in temperature at either very warm-wet or cold-dry sites. Sites that receive intermediate amounts of precipitation are more ambiguous, although spatial clustering of MIS 1–2 vs. MIS 3–5 advances is suggestive of past variations in precipitation at these sites. In western Tibet, no spatial or climatic correlation is observed with the timing of maximum glacial advances. We suggest this could arise from mis-interpretation of disparate boulder ages generated by a prolonged MIS-3/4 glacial advance in the western HKTP.

1. Introduction

Glaciers on the Himalaya–Karakoram–Tibet Plateau (HKTP) span a wide range of climatic conditions, from temperate maritime glaciers in the south and east, to dry-cold continental glaciers in the north and west. This variability is due to topography and to the climatic influences of the East Asian and Indian Monsoons in the east and south, and the mid-latitude westerlies, and Siberian high-pressure systems to the west and north (Benn and Owen, 1998; Rupper et al., 2009; Scherler et al., 2010; Seong et al., 2007). Because glacial chronologies are the most ubiquitous and easily accessible climate proxy on the HKTP, they hold a potentially useful record of how these climate systems changed over time. Cosmogenic nuclide dating of moraines has recently expanded the number of well-dated moraine sequences available on the HKTP, revealing that glacial advances throughout the HKTP are asynchronous (Chevalier et al., 2011; Heyman et al., 2011a; Owen et al., 2010, 2012). For example, many glaciers in the HKTP interior experienced maximum advances during Marine Isotope Stage (MIS) 3 or 4 (~73–28 ka), whereas many glaciers on the HKTP margins peaked during MIS-2 (~28–12 ka). The paleoclimatic interpretation of this asynchroneity remains unclear. Recent studies have proposed a range of explanations, calling upon changes in the strength of climatic systems (e.g. Benn and Owen, 1998; Owen et al., 2005), temperature variations (e.g. Rupper et al., 2009; Shi, 2002), topographic/hypsometric differences between neighboring catchments (Derbyshire, 1996; Owen et al., 2005), or a combination of several climatic parameters acting at different timescales (Scherler et al., 2010).

An alternative explanation for regional asynchroneity in some parts of the HKTP is incorrect interpretation of cosmogenic boulder ages. Most MIS-3/4 moraines in arid parts of the HKTP yield wide-ranging cosmogenic boulder ages, making it difficult to assign a mean age to each moraine (e.g. Chevalier et al., 2011; Hedrick et al., 2011). Variability in boulder ages is often attributed to post-depositional moraine degradation, implying that older boulder ages are more likely to record the timing of maximum glacial

* Corresponding author. Tel.: +1 802 443 5988.
E-mail address: wamidon@middlebury.edu (W.H. Amidon).

0012-821X/$ – see front matter
http://dx.doi.org/10.1016/j.epsl.2013.08.041

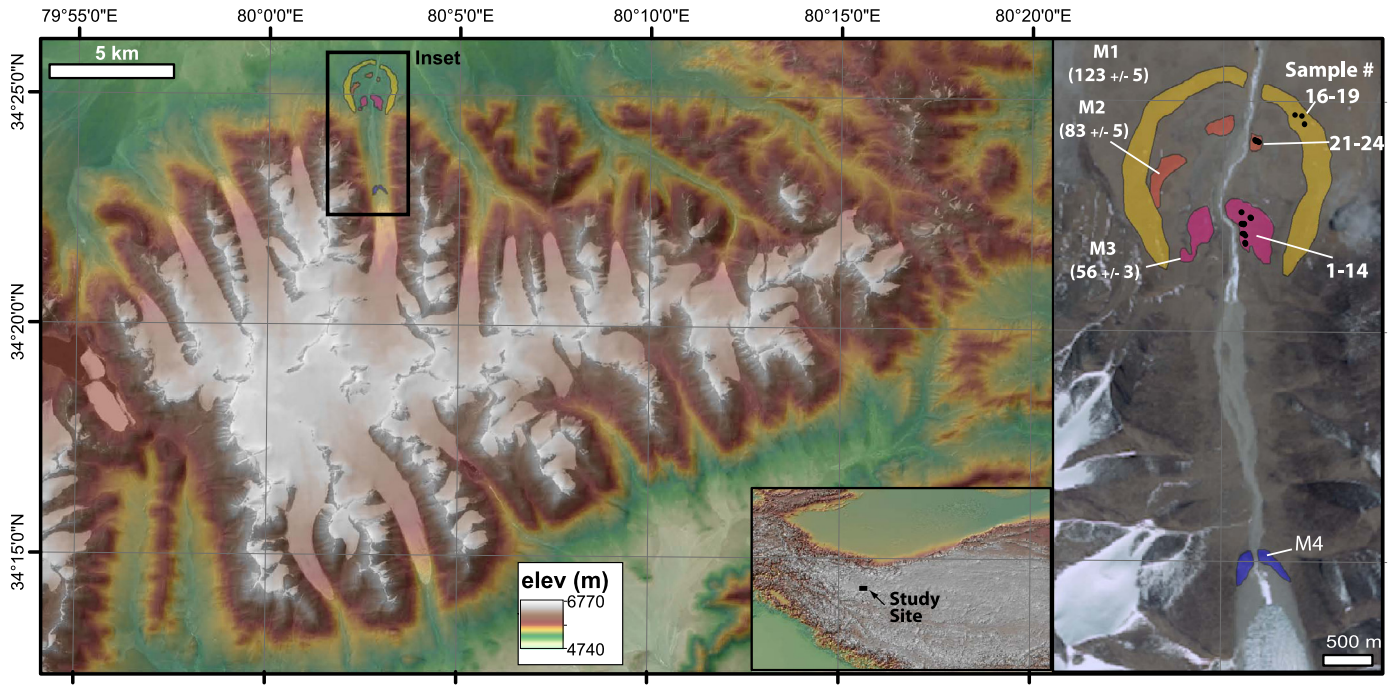

Fig. 1. Shaded-relief digital elevation model (DEM) of the Mawang Kangri range. Right panel shows close-up of Mawang Kangri (MK) ice cap and outlet glaciers on a SPOT-5 satellite image. The three-dated moraines are shown with 1σ age uncertainties. The highest moraine (M4) is the presumed, but yet undated, MIS-1/2 moraine near the glacier terminus.

advance (Heyman et al., 2011b; Putkonen and Swanson, 2003). In some cases, large age spreads may be related to glacial dynamics, such as the slow retreat of glacier termini in arid regions (Zech et al., 2005b). Thus, although testing asynchroneity requires robust moraine ages, it is possible that the quality of ages may be directly related to the climatic setting and mass balance response time of the glacier. Determining whether asynchroneity on the HKTP arises from paleoclimatic variations or poorly interpreted data is a difficult problem requiring additional well-dated moraine sequences and comparison with modern climatic data.

In this study we use in-situ cosmogenic ^{10}Be and ^{21}Ne dating of moraine boulders to develop a glacial chronology from the Mawang Kangri (MK) range in western Tibet (Fig. 1). Although the timing of advances (~123, 83, and 56 kyr) agrees well with some nearby sites, they do not match advances elsewhere in the western HKTP, suggesting asynchroneity. This may be partially because the MK site is one of the highest, coldest, driest, and most interior sites yet dated on the HKTP (glacial terminus at 5445 m asl). To understand the apparent asynchroneity, we perform a spatiotemporal analysis of maximum glacial advances on the entire HKTP. We explore two spatiotemporal cases of asynchroneity. First, we confirm the HKTP-wide asynchroneity mentioned above by showing maximum advances at interior and western sites occurred during MIS-3–5, earlier than maximum MIS 1/2 advances at many sites along the margin of the HKTP (Owen et al., 2005, 2002). Second, a western-HKTP asynchroneity is shown by the disagreement between the timing of MIS-3/4 advances at sites within the western HKTP. We explore the spatiotemporal dynamics causing these two cases by extracting modern precipitation, temperature, and topography data at well-dated glacial sites. We interpret the data in the context of two end-member hypotheses. First, does asynchroneity reflect unique local responses to broad-scale systematic changes in climatic forcing (e.g., temperature) across the entire HKTP? Alternatively, is asynchroneity caused by changes in the spatial pattern of precipitation or temperature over time? Our four main findings are: (1) the HKTP-wide asynchroneity can be explained by local responses to a systematic drop in temperature at end-member warm-wet and cold-dry sites; (2) advances at intermediate precipitation sites may reflect changes in spatial patterns of precipitation during MIS-1/2; (3) apparent western HKTP asynchroneity cannot be explained by either hypothesis, and may arise from the effects of prolonged glacial advances on moraine stability; and (4) topography does not exert a first order control on the timing of maximum glacial advances on the HKTP.

2. Geographic and climatic setting

2.1. Mawang Kangri (MK) field site

The MK mountain range sits in the far western interior of the Tibetan Plateau, consisting of several ~6400 m high peaks protruding above a small ice cap, which feeds multiple incised glacial valleys (Figs. 1 and 2). This study focuses on an unnamed valley near 34.3°N and 80.1°E, with a drainage area of ~44 km^2, and ~916 m of relief between the modern glacial terminus at 5445 m and the highest peak at 6368 m. The accumulation zone is dominated by firn basins, with a mean slope of ~15°. The current glacier has an ELA of ~6090 m, based on evaluation of the snow line in satellite imagery from August and September 2004, 2009, and 2010 (SPOT and WorldView imagery accessed via Google Earth). The oldest moraine (M1) is a semicircular piedmont moraine crest, reaching a minimum elevation of ~5300 m and sparsely adorned with large (>1.5 m) moraine boulders. The intermediate moraine (M2) is a terminal moraine fragment ~380 m upstream from M1, reaching ~5285 m elevation and adorned with smaller, ~0.5 m dimension boulders. The youngest dated hummocky moraine (M3) covers ~0.2 km^2, defined by a sharp southern edge, giving way to a low-relief surface with several hummocky crests. We interpret this deposit as having formed during a period of glacial stagnation, characterized by minor retreats and advances, and deposition of a large sediment load. A younger, undated terminal moraine (M4) is found ~3.5 km upstream from M3, ~0.58 km from the toe of the modern glacier.

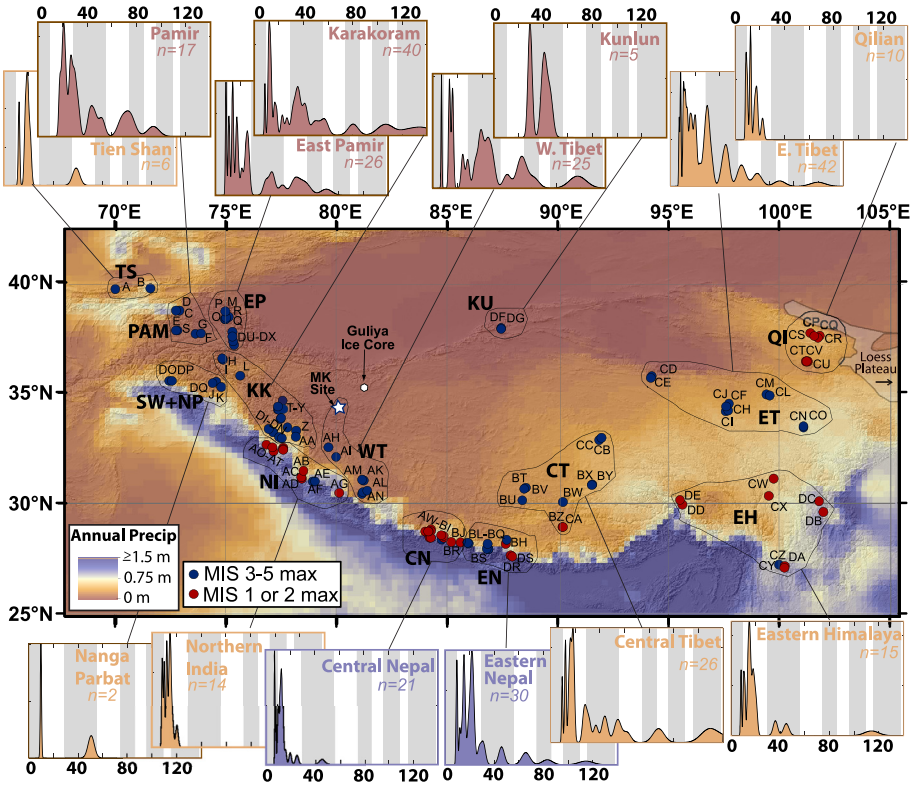

Fig. 2. Mean annual precipitation from 1998–2007 based on APHRODITE data (Yatagai et al., 2012). Dots represent glacial valleys classified by the timing of their maximum advance based on published work summarized in Heyman et al. (2011b). Sites have been grouped into regions based on geographic proximity and timing. The Mawang Kangri (MK) site is denoted by a white star. Graphs show probability density functions (PDFs) of 1σ filtered moraine ages (*not boulder ages*) found within each region from the dataset of Heyman et al. (2011b). PDF colors mimic the precipitation color-scale: ochre PDFs denote arid regions (<300 mm/yr), purple denotes high-precipitation regions (>900 mm/yr), and beige denotes intermediate regions. Grey and white bars denote Marine Isotope Stages 1–5e (Shackleton, 2000). Regions are abbreviated as: TS: Tien Shan, PAM: Pamir, EP: East Pamir, SW: Swat, NP: Nanga Parbat, KK: Karakoram, NI: Northern India, WT: Western Tibet, KU: Kunlun, CN: Central Nepal, EN: Eastern Nepal, CT: Central Tibet, ET: Eastern Tibet, QI: Qilian Shan Region, EH: Eastern Himalaya. (For interpretation of the references to color in this figure legend, the reader is referred to the web version of this article.)

2.2. Regional modern and paleoclimatic conditions

Mean annual temperatures at glacial termini across the HKTP are largely controlled by elevation and proximity to the ocean, ranging from ~−11 to 11 °C (Rodell et al., 2004). The monthly mean annual temperature at the terminus of the paleo-MK glacier (5305 m) is −11 °C, with mean temperature exceeding 0 °C only in July and August (Rodell et al., 2004). Temperatures during the global last glacial maximum (LGM) were likely ~4–9 °C cooler in the Tibetan interior (Bush, 2004; Shi, 2002; Shin et al., 2003), whereas Indian Ocean sea surface temperatures were probably only ~2 °C cooler (De Deckker et al., 2003; Shin et al., 2003).

Topographic barriers create a wide range of precipitation (~50 to 3000 mm/yr) on the HKTP, including desert conditions across much of the interior (Figs. 2 and 3). The MK site receives ~79 mm/yr of precipitation: ~80% in summer (JJAS), ~11% in winter (JFMA), and ~2% in fall (OND) (Yatagai et al., 2012), similar to other high-elevation sites on the Tibetan Plateau (Bookhagen and Burbank, 2010).

Precipitation across the HKTP is generated by three climatic systems, which play different roles depending on the season (Fig. 3). During the summer, onshore monsoonal winds create intense rain and snowfall in the "monsoon-influenced" southern and eastern regions of the HKTP, whereas summer westerlies bring little precipitation to the HKTP (Benn and Owen, 1998). During winter, the situation reverses as cold dry monsoon winds flow off the plateau, creating arid winters across much of the central, eastern, and southern HKTP. Winter westerlies trend further south in winter, delivering snowfall to the western regions of the HKTP. Winters in the northeastern HKTP are influenced by the Siberian high-pressure system, which encroaches on warm air masses in southern China, generating snowfall along the northeastern flank of the HKTP (Gong and Ho, 2002; Zhang et al., 2009).

Numerical modeling and proxy data give insight into how the four major climatic systems differed during the late Pleistocene. First, the east Asian monsoon system was driven by changes in insolation, with maxima at ~34 (MIS-3) and ~11 kyr (MIS-1) corresponding to wet periods in monsoon-influenced HKTP, and the insolation minimum at ~22 kyr (LGM) associated with drier conditions (Fang, 1991; Herzschuh, 2006; Prell and Kutzbach, 1992; Wang et al., 2008). However, several models predict that LGM monsoon precipitation may have increased in the southeast Himalaya due to the interaction of stronger south-westerly winds with northward flow generated by enhanced low-level convergence over Indonesia (Bush, 2004; Kim et al., 2008).

Second, although little observational data exists regarding past behavior of the westerlies, models predict southward deflection and increasing interaction with the HKTP (Bush, 2004; Ono and Irino, 2004). However, because global temperatures were colder during MIS-2, lower evaporative fluxes from Eurasia probably caused lower moisture contents in westerly air masses. Climate proxies from Aksayqin and Qarhan lakes in the western HKTP, show that MIS-2 was mostly dry, sandwiched between periods with high wetness in late MIS-3 and early MIS-1. Likewise, oxygen isotopes from the Guliya ice cap (western HKTP), suggest that MIS-1 and -3 were warm (and thus wet) intervals (Thompson et al., 1997).

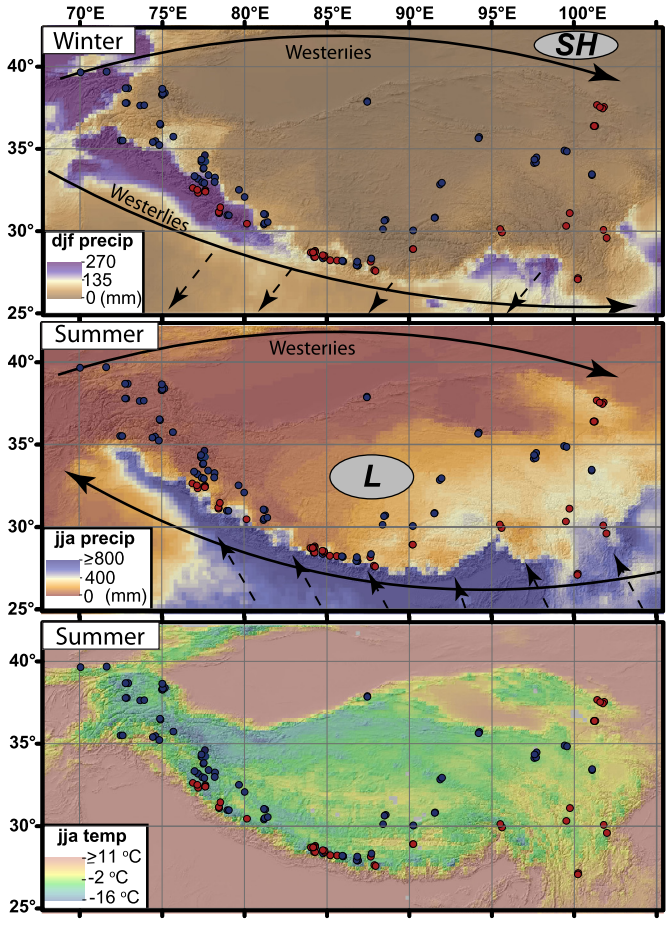

Fig. 3. Precipitation for northern hemisphere winter (top panel), summer (middle panel), and summer temperatures (bottom) based on APHRODITE and GLDAS respectively (Rodell et al., 2004; Yatagai et al., 2012). Bold arrows denote schematic atmospheric circulation patterns at ~3000 m elevation and dashed arrows represent circulation at ~500 m. "L" denotes Tibetan low-pressure center, and "H" denotes the southern edge of the Siberian high-pressure system.

Third, climate models suggest the Siberian high pressure system (Fig. 3; top panel) was strengthened during MIS-2, causing intensified frontal interactions along the northeastern HKTP. This may have pushed the desert margin of the Loess plateau (Fig. 2) further to the southeast, and increased moisture in the Qilian/Qinghai region during MIS-2 (Bush, 2004; Ding et al., 1999).

Changes in the relative strength of precipitation as a function of insolation are often invoked to explain the observed asynchroneity of glacial advances on the HKTP. Specifically, stronger summer insolation enhances seasonal heating over the HKTP, generating low air pressure and strengthening monsoon circulation (Kutzbach, 1981). For example, large MIS-1/2 advances along the margins of the HKTP are often attributed to a strengthened monsoon near the 11-kyr insolation peak. Likewise, a weak interior advance during the global LGM has been attributed to drier conditions near the 22-kyr insolation minima (Lehmkuhl and Owen, 2005; Owen et al., 2005). A large MIS-3 advance in the interior is thought to be driven by a prolonged monsoon associated with high summer insolation from ~60 to 35 kyr (Shi et al., 2001). However, several studies have pointed to the importance of temperature in controlling glacial advances on the HKTP. Shi (2002) suggest that severe cold and associated lack of precipitation during LGM time (early MIS-2) precluded large advances in the interior. Likewise, model results suggest that large MIS-1/2 advances along the margins of the Himalaya were largely driven by a drop in temperature due to enhanced cloud cover and reduced radiative forcing (Rupper et al., 2009).

3. Geochronology at the Mawang Kangri (MK) site

3.1. Geochronology methods

We sampled 21 granodiorite boulders for cosmogenic ^{10}Be and ^{21}Ne dating (Fig. 1; Table DR1). 2–3 cm thick samples were collected with a hammer and chisel, from which quartz was purified following standard laboratory procedures (Kohl and Nishiizumi, 1992). Purity of quartz was verified by ICPMS measurements of Al, which yielded concentrations of <100 ppm in all samples. ^{10}Be extraction was performed following published procedures in Bodo Bookhagen's lab at UCSB (Bookhagen, 2012; Bookhagen and Strecker, 2012). ^{10}Be measurements were made at Lawrence Livermore National Laboratory, following published procedures (Rood et al., 2010). ^{21}Ne measurements were made at Caltech, following identical procedures to those described in Amidon and Farley (2012). For reference, the same analytical techniques and instrument calibration yielded a cosmogenic ^{21}Ne concentration of 338 ± 10 Mat/g on the CRONUS-A quartz standard, in excellent agreement with the reported value of 333 ± 3 Mat/g (Balco and Shuster, 2009).

3.2. Geochronology results

Measured ^{21}Ne and ^{10}Be are in reasonable agreement with the ratio predicted by their production rates (Fig. DR2; Table 1, DR2, and DR3). Measured neon is generally a two-component mixture of air and spallation derived neon (Fig. DR1). Air components are large, with low ^{21}Ne/^{20}Ne ratios between ~0.0035 and 0.009, accounting for 30–85% of measured ^{21}Ne. ^{21}Ne concentrations in excess of air (^{21}Ne$_x$) are high, ranging from 25 to 60 Mat/g, with generally higher concentrations measured in samples from stratigraphically older moraines. Measured ^{10}Be ratios range from 1.4×10^{-11} to 7×10^{-12}, corresponding to concentrations of 2.4–11.6 Mat/g. Analytical uncertainties range from ~0.5 to 1.5% (Rood et al., 2013) and the ^{10}Be laboratory blank ($n = 3$) for these samples had a ^{10}Be/^{9}Be ratio of 2.8×10^{-14}.

Co-hosted ^{10}Be and ^{21}Ne concentrations allow cross-validation of the measurements and comparison with published production-rate ratios. Given that the moraine boulders have young (<150 kyr) simple exposure histories, we compare measured ^{10}Be/^{21}Ne ratios directly with production-rate ratios, neglecting the loss of ^{10}Be by decay, which should be less than a 5% effect. A weighted total least-squares regression (Fig. DR2) and a separate numerical mean of our data yield ^{10}Be/^{21}Ne of 0.19 ± 0.08 and 0.20 ± 0.03 respectively. This ratio is lower than two global calibrations of the ^{10}Be/^{21}Ne production-rate ratio, which both yielded ~0.23 (Goethals et al., 2009; Kober et al., 2011). It is also below the mean ^{10}Be/^{21}Ne of 0.27 ± 0.04 reported from ~4000 m in the eastern HKTP (Strasky et al., 2009). In contrast, our ^{10}Be/^{21}Ne ratio matches mean ratios recomputed from two high-elevation sites on the central HKTP: 0.20 ± 0.07 from ~4100 m (Schafer et al., 2008), and 0.19 ± 0.04 from ~5000 m (Strobl et al., 2012). These results suggest that the ^{10}Be/^{21}Ne production-rate ratio at high elevation in west-central HKTP is lower than the global average, consistent with unexpectedly low ^{10}Be/^{3}He ratios observed in the central Himalaya (Amidon et al., 2008; Gayer et al., 2004).

We adopt a ^{10}Be production rate calibrated for New Zealand (De = 3.88 ± 0.08 and Lm = 3.75 ± 0.08 at/g/yr), because this is the closest high-quality calibration site (Putnam et al., 2010). We then use the weighted mean ^{10}Be/^{21}Ne ratio of our own samples combined with the nearby results of Schafer et al. (2008),

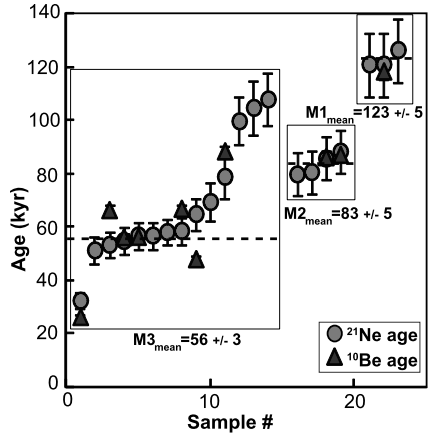

Fig. 4. Cosmogenic ^{21}Ne and ^{10}Be ages of boulders on three moraines (M1, M2 and M3) from the Mawang Kangri site shown with 1σ uncertainties. Ages are scaled using the Lal/Stone time-variable model with SLHL reference production rates of 3.75 and 18.7 at/g/yr for ^{10}Be and ^{21}Ne, respectively. Shielding and erosion are neglected.

(^{10}Be/^{21}Ne$_{mean}$ = 0.201 ± 0.011) to compute ^{21}Ne production rates (De = 19.35 ± 1.1 and Lm = 18.7 ± 1.1 at/g/yr). This choice of production rates satisfies our observed ^{10}Be/^{21}Ne ratio, and matches recently published results (Kober et al., 2011). ^{10}Be ages in Table 1 are reported using the Cronus online calculator v.2.2 (Balco et al., 2008), using the calibration dataset of Putnam et al. (2010). ^{21}Ne ages in Table 1 are computed using scaling factors derived from the Cronus calculator (Table 1), combined with the production rates stated above. As shown in Table 1, the Desilets (De), Dunai (Du), and Lifton (Li) scaling models agree to within 4% in western Tibet, whereas scaling factors from the Lal/Stone time variable model (Lm) are ~15% lower for older ages. All cosmogenic ages are discussed in terms of the Lal/Stone time-variable model (Lm).

^{21}Ne exposure ages from the older moraines M1 and M2 show tightly clustered ages (Table 1 and Fig. 4). Three ages from the oldest M1 moraine cluster at 123 ± 5 kyr (all uncertainties are 1σ). The mean of four samples from M2 cluster at 83 ± 5 kyr. In contrast, ages from the M3 hummocky surface scatter from 32 to 108 kyr, with a cluster of ages between 50–60 kyr. We assign an age of ~56 ± 3 kyr to M3 based on the mean of 7 samples clustered between 50–60 kyr, whose error bars overlap one another. In summary, we argue that the largest recent advances all occurred at or before ~56 kyr, whereas younger MIS-1/2 advances (presumably recorded by moraine M4) were confined close to the modern ice margin. This is consistent with the limited LGM advance at the nearby Guliya ice cap (Fig. 2), whose terminal moraine dated at 15.3 kyr sits only 50 m from the current ice margin (Yao et al., 1992).

4. Spatial analysis methods and results

4.1. Establishing timing of maximum glacial advances

To understand the cause of asynchroneity between MK and other sites on the HKTP, we compared its climatic and topographic characteristics with other well-dated glacial chronologies. We used the dataset of rescaled cosmogenic ages published by Heyman et al. (2011b), and added data from six additional chronologies (Damm, 2006; Owen et al., 2012; Richards et al., 2000a, 2000b; Taylor and Mitchell, 2000; Tsukamoto et al., 2002). We first estimate the age of each moraine by discarding 1σ outliers from the mean age, and then re-computing the mean age (1σ filtered mean

Table 1
Sample ages.

#	^{10}Be (Mat/g)	1σ (Mat/g)	^{21}Ne (Mat/g)	1σ (Mat/g)	Scaling factors					De		Lm		De		Lm	
					St	De	Du	Li	Lm	^{21}Ne age (kyr)	1σ (kyr)	^{21}Ne age (kyr)	1σ (kyr)	^{10}Be age (kyr)	1σ (kyr)	^{10}Be age (kyr)	1σ (kyr)
1	2.4	0	14.5	2.6	22.5	26.8	26.7	25.3	24	29	3	32.3	3	23	0.5	26	0.6
2	–	–	24.6	1	21.9	30.1	30.8	28.5	25.7	44	5	51.2	5	–	–	–	–
3	6.4	0.1	25.8	0.5	22.5	31.4	32.4	30	25.9	44	5	53.3	5	54	1.4	66	1.8
4	5.5	0.1	26.8	1.7	22.3	30.5	31.3	28.9	26.2	47	5	54.7	6	45	1.1	56	1.3
5	5.5	0.1	27.6	1.4	22.1	30.3	31	28.7	26	49	5	56.8	6	45	1.2	56	1.5
6	–	–	27.7	0.9	22.5	31.3	32.1	29.8	26.1	47	5	56.8	6	–	–	–	–
7	–	–	28.0	0.6	22.2	31	31.9	29.5	25.8	48	5	58.0	6	–	–	–	–
8	6.4	0.1	28.0	1	22.2	31	32	29.7	25.6	48	5	58.5	6	54	1.3	67	1.6
9	4.7	0.1	31.5	0.5	22.4	29.5	30.2	27.9	26	57	6	64.8	7	40	1.0	48	1.2
10	–	–	32.8	0.6	22	30.5	31.8	29.6	25.3	58	7	69.3	7	–	–	–	–
11	8.4	0.1	38.3	4.5	22.5	30.7	31.7	29.5	26	67	8	78.8	8	71	1.8	88	2.2
12	–	–	47.5	0.6	22.1	30.5	31.7	29.3	25.5	83	9	99.6	10	–	–	–	–
13	–	–	49.9	0.5	22.1	30.6	31.8	29.4	25.5	87	10	104.6	11	–	–	–	–
14	–	–	51.4	1.2	22.1	30.6	31.8	29.3	25.5	90	10	107.8	11	–	–	–	–
16	–	–	37.7	0.3	21.9	29.8	30.8	28.7	25.3	68	8	79.7	8	–	–	–	–
17	–	–	37.8	0.7	21.7	29.8	30.7	28.5	25.1	75	8	80.5	9	–	–	–	–
18	8.1	0.1	41.3	1	22.3	30.5	31.6	29.4	25.8	72	8	85.6	9	70	1.7	86	2.1
19	8.1	0.1	41.9	2.8	22	30.1	31.1	29	25.4	75	8	88.2	9	70	1.6	87	2.0
21	–	–	57.9	1.4	21.8	30.1	31.4	29	25.6	103	12	120.9	13	–	–	–	–
22	11.5	0.1	58.1	0.5	22	30.4	31.7	29.3	25.7	102	12	120.9	13	97	2.2	118	2.7
23	–	–	60.0	0.9	21.5	29.7	30.9	28.5	25.4	108	12	126.3	13	–	–	–	–

in appendix Table 3). Although this approach does not give preference to older ages (e.g. Heyman et al., 2011b), it is the most robust method to compare moraines across a wide range of ages and climatic regimes, without risk of mis-categorizing a moraine based on a single erroneous boulder age. Because resultant moraine ages vary widely, we assign them broadly to marine isotope stages (MIS): MIS-3/4 (73–28 kyr), MIS-2 (28–12 kyr), or MIS-1 (<12 kyr) (Shackleton, 2000). After assigning an MIS stage to each moraine in a given valley, we then classified each valley based on when the maximum glacial advance occurred (Table DR4). This classification was undertaken based on the maps and written analysis presented in each of the published papers, supplemented by visual inspection of geomorphic relationships using satellite imagery in Google Earth. Each valley in the dataset meets three basic criteria: (1) multiple documented moraines in the valley, (2) at least one well-dated moraine per valley, and (3) evidence that the authors looked carefully for other moraines and assigned absolute or relative ages to all moraines present. Finally, each site is assigned a confidence criteria reflecting the degree of confidence in classification at each site (Table DR4).

The main strength of this approach is that it capitalizes on a large number of recent studies that have expanded the spatial extent and temporal resolution of glacial chronologies. Although some classifications are uncertain, the large dataset reveals meaningful first-order trends. By focusing on the relative sizes of recent advances in each valley, our approach avoids the complex process of computing equilibrium line altitudes for past advances. Instead, the approach effectively normalizes for the complicating factor of topography, which can be assumed constant (to the first order) over the last 150 kyr, thereby amplifying the signal of regional changes in precipitation and temperature over time.

One weakness of this approach is the possibility that authors missed evidence of specific advances. However because most studies involve detailed field observation and mapping we consider moraine omission to be a minor source of uncertainty. A second weakness is the issue of low moraine preservation potential in rapidly eroding valleys, particularly along the temperate Himalayan front where erosion rates are high (Owen et al., 2005). For example, highly eroded glacial remnants are briefly mentioned but not dated at certain sites in northern India and central Nepal (Owen et al., 2001; Pratt-Sitaula, 2004). However, other sites in the temperate frontal Himalaya show well preserved MIS-3/4 moraines (Abramowski, 2004; Kong et al., 2009). Although preservation issues are worthy of further study, they are unlikely to undermine the results presented here due to the large number of diverse sites included in the dataset.

The most striking result of our analysis of maximum advances is the strong spatial clustering of MIS-3+ vs. MIS-1/2 advances, which we divide into 14 regions based on spatial proximity and timing of advance (Fig. 2). The observed "HKTP-wide asynchroneity" is consistent with previous observations: maximum MIS-1/2 glaciations occur mostly near the margins of the HKTP, whereas interior and western regions are devoid of strong MIS-1/2 advances (Owen et al., 2002). The MK site is grouped together with other sites in the "western Tibet" region, all of which show maximum advances during MIS-3+.

4.2. Precipitation and temperature analysis

Monthly precipitation data from 1998–2007 were extracted at 0.25° resolution from the Aphrodite V1003R1 data set (Yatagai et al., 2012). The relatively short time window encompassed by these data trades off against excellent spatial resolution and improved reliability over remote areas with sparse land-based measurements. Because remotely-sensed snowfall data are subject to high uncertainties, we use mean spring (MAMJ) snow cover as a proxy for winter snowfall instead. We chose these four months as a window when snow cover would be most sensitive to accumulated winter snow pack and less sensitive to peak summer temperatures. Snow cover data from 2000–2012 was extracted from the MODIS/Terra L3 8-day snow cover product (MOD10C2) by averaging nine 0.05 degree pixels at each site (Hall et al., 2012). Monthly mean temperature from 2000–2012 was extracted at 0.25° resolution from the Global Land Data Assimilation (GLDAS) version 1 dataset (Rodell et al., 2004). Temperatures at different elevations within the watershed were computed by applying a 5.5 °C/km lapse rate relative to the elevation and temperature assigned to the model cell in the GLDAS data. This number recognizes that typical summer lapse rates on the HKTP are ~5.5 °C/km, with generally lower rates in winter months, and higher rates in summer (Feng et al., 2011; Joshi and Ganju, 2010). Positive degree months (pdm) are computed by first calculating the monthly average temperatures at the moraine terminus for the period 2000–2012, then summing the total degrees above zero across the 12 months (excluding negative mean temperatures). For example, if July and August have mean temperatures of 4 and 6 °C, and are the only monthly means above zero, then the pdm is 10 °C/yr.

A major result of our climatic analysis is that sites within each region share similar annual precipitation values but differ widely in temperature (Fig. 5). Importantly, all arid sites (<300 mm/yr in Fig. 5) experienced maximum MIS-3+ advances regardless of temperature, suggesting that precipitation is the most important forcing factor at these sites. In contrast temperature appears to be the most important variable at high-precipitation sites (>900 mm/yr) because most warm high-precipitation sites show MIS-1/2 advances, whereas many cold high-precipitation sites show MIS-3+ advances. Regions of moderate precipitation show a more complex behavior with a random mix of MIS-2 and MIS-3+ maximum advances and no clear dependence on either precipitation or temperature.

We further discriminate regions based on seasonality of precipitation by plotting summer (JJA) precipitation against spring snow cover. Many sites on the western HKTP, and all sites on the eastern HKTP receive weak winter snowfall, expressed as low spring snow-cover (Fig. 6). In contrast, the MK site and sites in the Pamir and *western* Karakoram have high snow cover due to high elevation and capture of eastward moisture transport. Northern India is a unique region that receives both strong winter snowfall and moderate summer monsoon precipitation.

4.3. Topographic analysis

Elevation distributions were extracted from void-filled SRTM 90-m DEM (http://www.viewfinderpanoramas.org), using watersheds defined relative to the lowest elevation dated moraine in each valley. Minimum, median and maximum elevation were computed, along with mean 5-km relief and mean slope above the median elevation. Normalized hypsometries and two different hypsometric metrics were also computed: (1) the hypsometric integral (HI) reflects the area under the curve and is lower in watersheds whose surface area is skewed towards lower elevations by intense glacial erosion (Brocklehurst and Whipple, 2004), and (2) the hypsokyrtome (Hkr) is the normalized elevation at which the slope of the hypsometric line first exceeds a reference slope (1.5 in this case). Larger Hkr values reflect that the watershed has been more intensely modified by glaciation, driving it towards a "u-shaped" rather than "v-shaped" morphology (Sternai et al., 2011).

Hypsometric and topographic data show no relationship with the timing of maximum advances (Fig. 7 and DR3). For example, the Karakoram, western Tibet, and northern India regions have nearly identical hypsometric properties (HKr and HI), but show completely different maximum advances (Fig. 7). Likewise no cor-

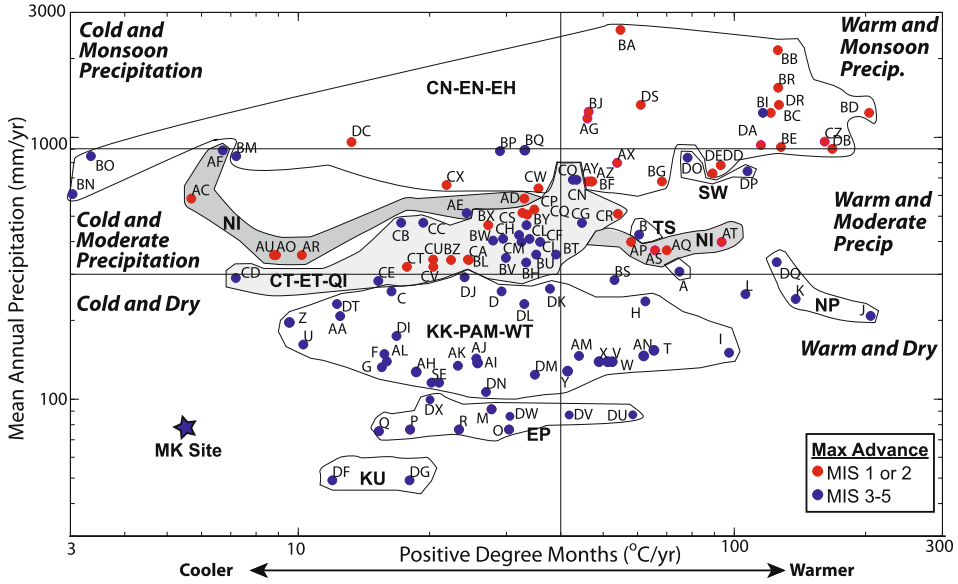

Fig. 5. Positive degree months (PDM) plotted against mean annual precipitation. Positive degree months are computed at the paleo-glacier terminus from the GLDAS/NOAH v1 dataset using a lapse rate of 5.5 °C/km. PDM are computed by first calculating the monthly average temperatures at the moraine terminus for the period 2000–2012, then summing the total degrees above zero across the 12 months (excluding negative mean temperatures). The log–log scale masks two orders of magnitude variation in both precipitation and temperature, which are arbitrarily divided into warm and cold regions based on the distribution of data. The geographic regions denoted in Fig. 2 are outlined where possible.

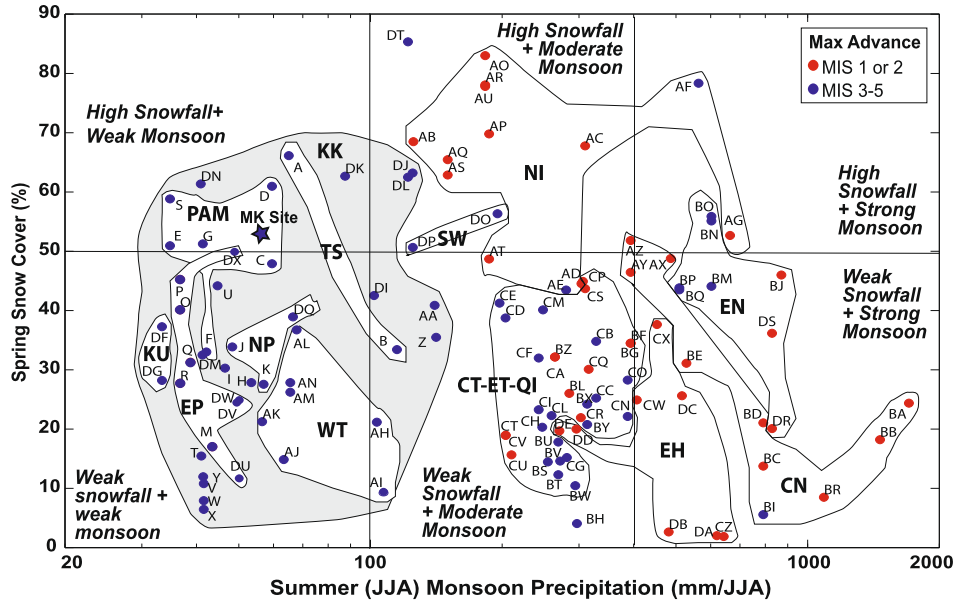

Fig. 6. Summer monsoon precipitation (June to August) plotted against spring snow cover (March to June) as determined from the MODIS 8-day snow cover product MOD10C2. Winter precipitation as expressed in percent snow-cover area is most significant in northern India and adjacent regions of the western Karakoram, whereas monsoon precipitation is most important in southern and eastern HKTP.

relation is observed between the timing of maximum advance and (1) the mean slope of the accumulation zone, or (2) mean 5-km relief of the accumulation zone (Fig. DR3b). For example, sites in northern India that all experienced maximum MIS-2/1 advances (AP–AU, AB–AD) span a large range of mean slopes (21–31°) and mean relief (1150–2050 m).

Considered spatially, our hypsometric results show that sites in the eastern HKTP have experienced more long-term (~3 Myr) glacial landscape modification than sites in the western HKTP. For example, 6 of the 7 highest hypsokyrtomes (HKr) occur in the eastern half of the study area, as do 3 of the 4 lowest hypsometric integrals (Fig. 7). The MK site exhibits an intermediate degree of glacial landscape modification (HI = 0.53; Hkr = 0.13) relative to the entire dataset (Fig. 7). However, MK stands out as strongly modified site when compared to nearby sites in the western HKTP (e.g., Karakoram and western Tibet).

5. Discussion

5.1. Evaluating HKTP-wide asynchroneity

The first finding of our analysis is that HKTP-wide asynchroneity can potentially be explained by locally variable responses to a systematic drop in temperature during MIS-1/2. We identify two end-member climatic regimes, which predict the timing of maximum advance (Figs. 2, 4, and 7). The first group includes cold-

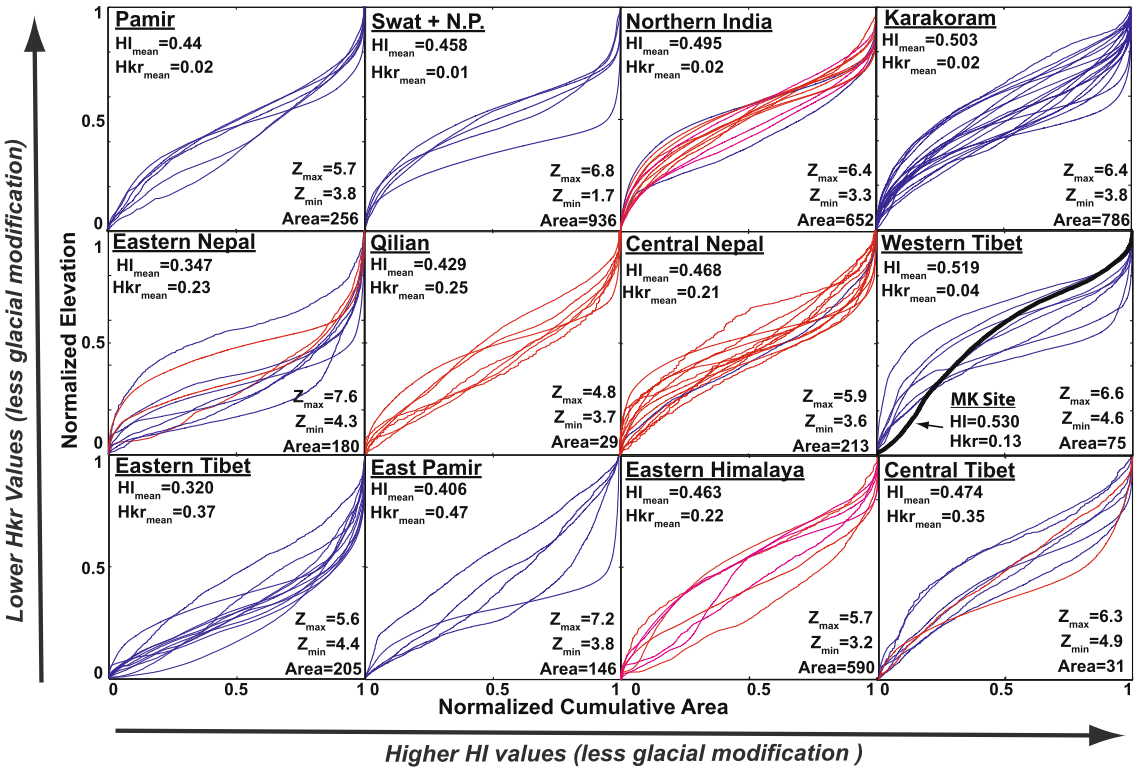

Fig. 7. Hypsometric integrals (HI) and hypsokyrtomes (HKr) are plotted for each region. Additionally, mean peak and terminus elevations (Z_{max} and Z_{min}) and mean hypsometric integrals are shown for each region. Data were extracted from void filled SRTM-90 m data. Blue lines denote sites with MIS-3–5 maximum advances, red lines denote MIS-1/2 maximum advances. (For interpretation of the references to color in this figure legend, the reader is referred to the web version of this article.)

dry interior sites, which are generally precipitation limited and show exclusively MIS-3+ maximum advances (Karakoram, Pamir, Western, Central, and Eastern Tibet). These sites likely experienced negative mass balances stemming from 6–8 °C cooler temperatures and associated summer snowfall reductions during MIS-2. The second group includes wet-warm sites on the margins of the HKTP, which are generally ablation limited and show mostly MIS-1/2 advances (central Nepal, sites DR and DS in eastern Nepal, and sites CZ–DE in eastern Himalaya). These sites likely experienced positive mass balances from a drop in temperature during MIS-2 through a reduction in melt-dominated ablation and increased summer snowfall. The different local responses to a drop in temperature during MIS-2 were likely magnified by the much larger temperature decrease at interior sites relative to marginal sites, which were buffered by warmer maritime air masses. Colder interior temperatures would strongly suppress precipitation at cold-dry interior sites, without greatly reducing sublimation-dominated ablation.

Further evidence that maximum advances in warm-wet regions were driven by a drop in temperature comes from sites in Nepal. Sites BM–BQ in eastern Nepal overlap geographically with sites in central Nepal (AX–BJ), and receive similar high-precipitation, yet they do not show maximum MIS-1/2 advances. These weak MIS-1/2 advances in eastern Nepal were generally restricted to cold high-elevation sites (BM–BQ) (Finkel et al., 2003; Schafer et al., 2008), where colder temperatures limited the benefit of an MIS-2 temperature drop. Thus, it appears that the timing of maximum advance in the wettest parts of the HKTP may be controlled by temperature, consistent with the findings of Rupper et al. (2009) and Scherler et al. (2010).

A second finding of our analysis is the possibility that patterns of precipitation during MIS-1/2 may have differed from today. This arises from considering a third group of intermediate precipitation sites (300–900 mm/yr and <40 pdm), which cannot easily be defined as precipitation or ablation limited. This intermediate group includes sites in five regions, which share similar modern climatic characteristics: (1) certain sites in the eastern Himalaya (CW–CX, DC), (2) Qilian Shan (CP–CU), (3) northern India (AC–AF and AP–AU), (4) eastern Tibet (CD–CO), and (5) central Tibet (BU–CC) (Figs. 2–4). Although more detailed study is required to predict exactly how these regions should have responded to cooler MIS-2 temperatures, they should have responded in broadly similar ways due to their climatic similarities. Instead, strong spatial clustering of maximum MIS-1/2 or MIS-3+ advances seems to dominate the signal, suggesting these advances were controlled by a spatially heterogeneous forcing. Given that patterns of precipitation are more likely to have changed in a heterogeneous way than temperature, we briefly speculate on possible paleo-precipitation scenarios.

First, strong MIS-2 advances at sites DC–DE, CW–CX, BZ–CA near the eastern Himalaya could be explained by strengthened summer monsoon precipitation in the southeast Himalaya during MIS-2, consistent with recent model results (Bush, 2002, 2004). Second, maximum MIS-2 advances in the Qilian Shan region may result from its unique location on the northeastern edge of the HKTP, where it would have benefited from low-level convergence created by a strengthened Siberian high-pressure system. This explanation is consistent with model results and observations suggesting the northeast desert margin of the Loess plateau was wetter during MIS-2 (Bush, 2004; Ding et al., 1999). Moreover, lacustrine records from this region show rapid warming and high precipitation during late MIS-2 (Colman et al., 2007; Herzschuh et al., 2006, 2005).

Third, northern India is unique because glaciers rely heavily on winter accumulation (Fig. 6). Because most sites experienced maximum MIS-1/2 advances independent of temperature, a source of enhanced precipitation is a plausible candidate for the strong MIS-1/2 advance. We speculate that maximum MIS-1/2 advances in northern India are driven by high winter snowfall sustained by

more frequent western disturbances during MIS-2. Western disturbances are synoptic surface low-pressure systems that move (north)eastward across the northern India region, often associated with a southward shift of the Asian jet stream and enhanced northward winds (Dimri, 2006; Yadav et al., 2006; Yadav, 2009). Given these conditions are thought to have characterized the southwest HKTP during MIS-2 (Bush, 2004), it seems plausible that western disturbances and thus winter snowfall was strengthened during MIS-2. This is further supported by lacustrine paleoclimatic archives from this region that indicate higher amounts of moisture flux with a western source region (Demske et al., 2009; Wünnemann et al., 2010).

5.2. Evaluating the western HKTP asynchroneity

Timing of advances at MK match the closest neighboring sites, but are apparently asynchronous with sites elsewhere in the western HKTP. For example, sites T–Y in the Ladakh range (Owen et al., 2006a), site Z in northern Zanskar (Hedrick et al., 2011), and sites AI–AH in the Ayliari range (Chevalier et al., 2011) all show strong discrete MIS-5e advances around 112–130 kyr (Table DR4). Likewise, the Ladakh range (T–Y) shows advances at ~80–85 kyr, and sites in Zanskar show advances near ~55 and 52 kyr (AA and Z). Fig. 8 shows that the timing of these advances are coincident with periods of elevated Indian monsoon activity, global warm periods recorded in the NGRIP ice core, and local warm periods recorded in the Guliya ice cap (Clemens and Prell, 2003; NGRIP Project, 2004; Thompson et al., 1997). This suggests that cold-dry interior glaciers respond positively to warmer and wetter conditions in the region. However, these advances are not perfectly in-phase with any of the proxies, and several optimal wet-warm periods, such as early MIS-1, are not recorded by an advance.

One explanation for the western HKTP asynchroneity during MIS-3/4 is past variations in climatic conditions across the region. We consider two end-member hypotheses related to climate: (1) do MIS 3/4 advances in the western HKTP reflect past spatial variations in patterns of precipitation or temperature, or (2) do they reflect locally modulated responses to broad systematic climate changes? To test these ideas we correlated the 1σ-filtered moraine ages with geographic location, climatic, and topographic parameters. The lack of spatial clustering of MIS-3/4 moraine ages (Fig. DR5) argues against the first hypothesis that MIS-3/4 advances were controlled by past spatial variations in climate. The lack of correlation with local precipitation, temperature, or hypsometry (Fig. DR4) argues against the second hypothesis that large advances are controlled by locally modulated responses to a systematic shift in climate conditions.

A second possible explanation for the western HKTP asynchroneity during MIS-3/4 is that low ice flux through cold-dry glaciers of the western HKTP leads to very slow glacial response times. The timing of max advances thus reflects climate changes modulated by local conditions superposed upon the time-averaged memory of past responses at that location (Rupper and Roe, 2008). Such conditions would create different phase shifts between optimal forcing conditions and the timing of maximum advance at each site, preventing simple correlation in geographic and climatic space. Long lag times are consistent with the very minor advance observed at MK and the nearby Guliya ice cap during mate MIS-2 and early MIS-1 (Yao et al., 1992). This may be explained by the relatively short time window during which optimum temperatures existed (~14–8 kyr), which was less than the response time of these arid interior glaciers. A simple test of this explanation can be made using the linear model for glacier length fluctuations (e.g. Roe and O'Neal, 2009). We adopt a melt factor of 3.45 mm/(°C day) and lapse rate of 4.5 °C/km reported for glaciers in nearby regions of western Tibet (Zhang et al., 2006), as well as measured

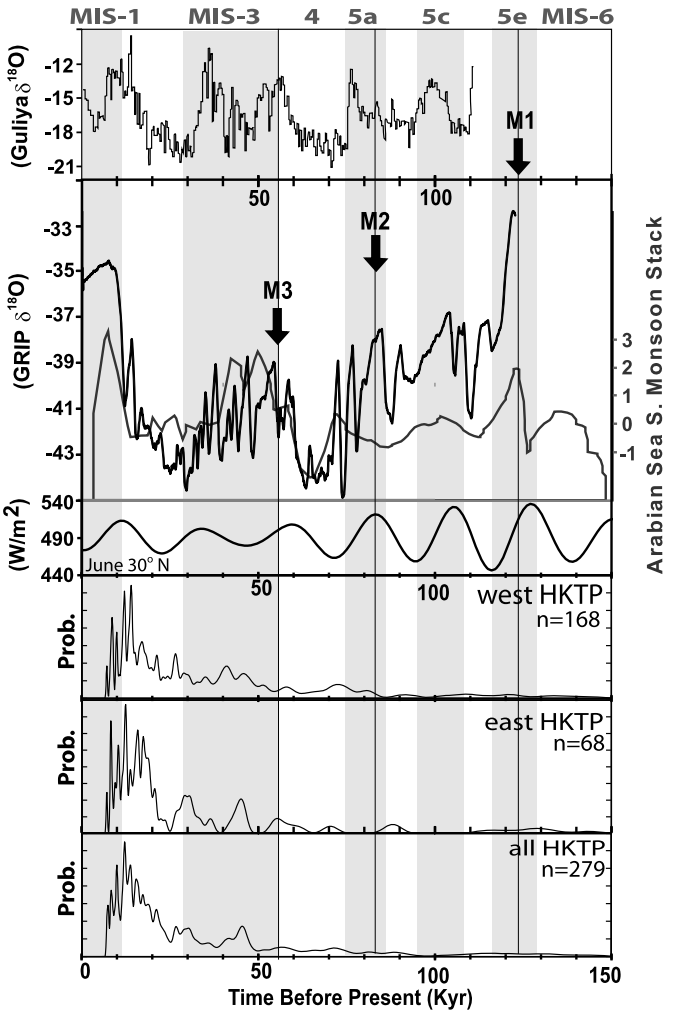

Fig. 8. Compilation of climate proxies compared with the timing of advances at Mawang Kangri (arrows with M1–M3), and marine isotope stages (shaded bands). The bottom three panels show probability density functions of 1σ-filtered moraine ages (*not boulder ages*) from the eastern HKTP (QI, ET, CT, and ETH), the western HKTP (TS, PAM, EP, KK, NP, WT, and NI), and the entire HKTP. The $\delta^{18}O$ records from the Guliya and NGRIP ice cores are taken as proxies for temperature at Mawang Kangri and in the northern hemisphere, respectively (NGRIP Project, 2004; Thompson et al., 1997). The Arabian Sea summer monsoon stack is taken as a proxy for the Indian monsoon intensity (Clemens and Prell, 2003). June insolation at 30°N is provided for Ref. Berger and Loutre (1991).

parameters for the Mawang Kangri glacier (slope = 0.04, width = 0.96 km, height = 0.235 km, area = 18.6 km^2, and ELA = 6090 m). These parameters yield an e-folding relaxation time (the time required for a glacier to return to its equilibrium state following a perturbation) of ~140 yr. Although this timescale is ~20 times longer than reported for temperate glaciers on temperate glaciers such as Mt. Baker (Roe, 2011), it is not long enough to account for lag times of several thousand years.

A third possible explanation for the western-HKTP asynchroneity is incorrect interpretation of pseudo-random moraine boulder ages resulting from a prolonged glacial advance across the region from ~35–60 kyr (Fig. 8). In this case, glaciers would have oscillated near their maximum extents for 20–30 kyr, reworking moraine surfaces and creating the high volume, multi-lobed, hummocky moraines observed at Mawang Kangri and elsewhere in the western HKTP (Zech et al., 2005b). This interpretation is consistent with the wide range of cosmogenic ages obtained from MIS-3/4 moraines in the western HKTP and underscores the relationship between local climate, mass-balance dynamics, and the distribution of boulder ages. Relatively rapid and short lived glacial ad-

vances may be a pre-requisite for successful cosmogenic dating of moraines.

5.3. Interpreting hypsometry and topographic parameters

Although topography plays a role in defining the length of ice advance under a given set of climatic conditions (cf. Lehmkuhl and Owen, 2005), it does not exert a first order control on the timing of maximum advance on the HKTP. This observation is consistent with recent studies, which show that glacier geometry does not exert a strong control on regional variations in glacier length changes (Huybers and Roe, 2009). By contrast, our hypsometric results clearly show that sites in the eastern HKTP have experienced more glacial landscape modification than sites in the western HKTP (Fig. 7). This first-order spatial relationship probably reflects the long-term importance of monsoon precipitation in driving high ice fluxes and intense glacial erosion. However, sites in the eastern-half of the HKTP do not show a direct correlation between precipitation and glacial modification. Instead, moderate precipitation sites in eastern and central Tibet show some of the most glacially modified landscapes. We interpret this to reflect the importance of tectonic uplift in dropping base level and accelerating river incision in landscapes along the margins of the HKTP (e.g., central Nepal). In such places the time integrated effects of fluvial incision sculpt the landscape more effectively than the periodic advances of large valley glaciers. The lack of correlation with drainage area suggests that these observations are not scale-dependent, and that they attest to the long-term stability of monsoon precipitation patterns on the HKTP.

6. Conclusions

We have developed a cosmogenic ^{10}Be and ^{21}Ne chronology of glacial advances at Mawang Kangri (MK) – one of the highest, coldest, and driest sites yet dated in the Tibetan interior. We estimate a ^{10}Be/^{21}Ne production ratio of 0.20 ± 0.07, slightly lower than the global average, but similar to previous high-elevation studies on the Himalaya–Karakoram–Tibet Plateau (HKTP). Good clustering of moraine ages shows discrete advances at ~123, 83, and a prolonged advance near 56 kyr, with only minor advances occurring during MIS-1/2. Large MIS-3+ advances at MK are probably driven by optimal combinations of warmth and monsoon intensity.

Our spatiotemporal analysis of glacial advances on the HKTP reveals two tiers of asynchroneity. First, "plateau-wide" asynchroneity is reflected by MIS-3+ advances at MK and other western/interior sites, relative to maximum MIS-1/2 along the margin of the HKTP. Second, a "western HKTP" asynchroneity is apparent between the ~56-kyr advance at MK and the timing of other MIS-3/4 maximum advances in the western HKTP. Our analysis suggests that the first order plateau-wide asynchroneity can be explained by locally variable responses to systematic cooling during MIS-2, particularly for the end-member regimes of either precipitation or ablation-limited glaciers. To the second order, variable MIS-1/2 advances in regions of intermediate precipitation suggest that past spatial variations in precipitation may be important in northern India, the eastern Himalaya, and the Qilian Shan region. The western-HKTP asynchroneity cannot be easily explained by past spatial variations in climate or local topography. Instead, we argue that apparent asynchroneity of MIS-3/4 advances may arise from widely distributed moraine ages generated by prolonged glacial advances during MIS-3/4.

Finally, our results suggest that although topography plays a role in defining the length of ice advance under a given set of climatic conditions, it does not influence the timing of regional ice advance and retreat on the HKTP. Sites with more intense monsoon precipitation show higher degrees of glacial erosion, suggesting that ice flux is the primary control on hypsometry and that the observed patterns of precipitation on the HKTP have not changed dramatically over the Pleistocene.

Acknowledgements

Thanks to Jing Liu for help with logistical arrangements, Ken Farley for use of his laboratory, and to Ed Amidon for field assistance. Reviews by Ben Laabs and an anonymous reviewer greatly improved the manuscript. Partial funding was provided by the Caltech Tectonics Observatory.

Appendix A. Supplementary material

Supplementary material related to this article can be found online at http://dx.doi.org/10.1016/j.epsl.2013.08.041.

References

Abramowski, U., 2004. The use of ^{10}Be surface exposure dating of erratic boulders in the reconstruction of the Late Pleistocene glaciation history of mountainous regions, with examples from Nepal and Central Asia. PhD thesis. University of Bayreuth, Bayreuth.

Amidon, W.H., Farley, K.A., 2012. Cosmogenic ^{3}He and ^{21}Ne dating of biotite and hornblende. Earth Planet. Sci. Lett. 313–314, 86–94.

Amidon, W., Farley, K.A., Burbank, D.W., Pratt-Sitaula, B., 2008. Anomalous cosmogenic ^{3}He production and elevation scaling in the high Himalaya. Earth Planet. Sci. Lett. 265, 287–301.

Balco, G., Shuster, D.L., 2009. Production rate of cosmogenic Ne-21 in quartz estimated from Be-10, Al-26, and Ne-21 concentrations in slowly eroding Antarctic bedrock surfaces. Earth Planet. Sci. Lett. 281, 48–58.

Balco, G., Stone, J.O., Lifton, N.A., Dunai, T.J., 2008. A complete and easily accessible means of calculating surface exposure ages or erosion rates from ^{10}Be and ^{26}Al measurements. Quat. Geochronol. 3, 174–195.

Benn, D.I., Owen, L.A., 1998. The role of the Indian summer monsoon and the mid-latitude westerlies in Himalayan glaciation: Review and speculative discussion. J. Geol. Soc. 155, 353–363.

Berger, A., Loutre, M.F., 1991. Insolation values for the climate of the last 10 million years. Quat. Sci. Rev. 10, 297–317.

Bookhagen, B., 2012. http://www.geog.ucsb.edu/~bodo/pdf/bookhagen_chemSeparation_UCSB.pdf.

Bookhagen, B., Burbank, D.W., 2010. Toward a complete Himalayan hydrological budget: Spatiotemporal distribution of snowmelt and rainfall and their impact on river discharge. J. Geophys. Res., Earth Surface 115 (F3).

Bookhagen, B., Strecker, M.R., 2012. Spatiotemporal trends in erosion rates across a pronounced rainfall gradient: Examples from the southern Central Andes. Earth Planet. Sci. Lett. 327–328, 97–110.

Brocklehurst, S.H., Whipple, K.X., 2004. Hypsometry of glaciated landscapes. Earth Surf. Process. Landf. 29, 907–926.

Bush, A.B.G., 2002. A comparison of simulated monsoon circulations and snow accumulation in Asia during the mid-Holocene and at the Last Glacial Maximum. Glob. Planet. Change 32, 331–347.

Bush, A.B.G., 2004. Modelling of late Quaternary climate over Asia: a synthesis. Boreas 33, 155–163.

Chevalier, M.L., Hilley, G., Tapponnier, P., Van der Woerd, J., Jing, L.Z., Finkel, R.C., Ryerson, F.J., Li, H.B., Liu, X.H., 2011. Constraints on the late Quaternary glaciations in Tibet from cosmogenic exposure ages of moraine surfaces. Quat. Sci. Rev. 30, 528–554.

Clemens, S.C., Prell, W.L., 2003. A 350,000 year summer-monsoon multi-proxy stack from the Owen ridge, Northern Arabian Sea. Mar. Geol. 201, 35–51.

Colman, S.M., Yu, S.Y., An, Z., Shen, J., Henderson, A., 2007. Late Cenozoic climate changes in China's western interior: A review of research on Lake Qinghai and comparison with other records. Quat. Sci. Rev. 26, 2281–2300.

Damm, B., 2006. Late Quaternary glacier advances in the upper catchment area of the Indus River (Ladakh and Western Tibet). Quat. Int. 154, 87–99.

De Deckker, P., Tapper, N.J., van der Kaars, S., 2003. The status of the Indo-Pacific Warm Pool and adjacent land at the Last Glacial Maximum. Glob. Planet. Change 35, 25–35.

Demske, D., Tarasov, P.E., Wünnemann, B., Riedel, F., 2009. Late glacial and Holocene vegetation, Indian monsoon and westerly circulation in the Trans-Himalaya recorded in the lacustrine pollen sequence from Tso Kar, Ladakh, NW India. Palaeogeogr. Palaeoclimatol. Palaeoecol. 279, 172–185.

Derbyshire, E., 1996. Quaternary glacial sediments, glaciation style, climate and uplift in the Karakoram and Northwest Himalaya; review and speculations. Palaeogeogr. Palaeoclimatol. Palaeoecol. 120, 147–157.

Dimri, A.P., 2006. Surface and upper air fields during extreme winter precipitation over the western Himalayas. Pure Appl. Geophys. 163, 1679–1698.

Ding, Z., Sun, J., Rutter, N.W., Rokosh, D., Liu, T., 1999. Changes in sand content of loess deposits along a north–south transect of the Chinese Loess Plateau and the implications for desert variations. Quat. Res. 52, 56–62.
Fang, J., 1991. Lake evolution during the past 30,000 years in China and its implications for environmental change. Quat. Res. 36, 37–60.
Feng, S., Fu, Y.F., Xiao, Q.N., 2011. Is the tropopause higher over the Tibetan Plateau? Observational evidence from Constellation Observing System for Meteorology, Ionosphere, and Climate (COSMIC) data. J. Geophys. Res., Atmos. 116.
Finkel, R.C., Owen, L.A., Barnard, P.L., Caffee, M.W., 2003. Beryllium-10 dating of Mount Everest moraines indicates a strong monsoon influence and glacial synchroneity throughout the Himalaya. Geology 31, 561–564.
Gayer, E., Pik, R., Lave, J., France-Lanord, C., Bourles, D., Marty, B., 2004. Cosmogenic ^{3}He in Himalayan garnets indicating an altitude dependence of the ^{3}He/^{10}Be production ratio. Earth Planet. Sci. Lett. 229, 91–101.
Goethals, M.M., Hetzel, R., Niedermann, S., Wittmann, H., Fenton, C.R., Kubik, P.W., Christl, M., von Blanckenburg, F., 2009. An improved experimental determination of cosmogenic ^{10}Be/^{21}Ne and ^{26}Al/^{21}Ne production ratios in quartz. Earth Planet. Sci. Lett. 284, 187–198.
Gong, D.Y., Ho, C.H., 2002. The Siberian High and climate change over middle to high latitude, Asia. Theor. Appl. Climatol. 72, 1–9.
Hall, D., Riggs, G., Salomonson, V., 2012. MODIS/Terra snow cover 8-day L3 global 0.05 deg CMG V005, 2000–2012. National Snow and Ice Data Center, Boulder, Colorado.
Hedrick, K.A., Seong, Y.B., Owen, L.A., Caffee, M.W., Dietsch, C., 2011. Towards defining the transition in style and timing of Quaternary glaciation between the monsoon-influenced Greater Himalaya and the semi-arid Transhimalaya of Northern India. Quat. Int. 236, 21–33.
Herzschuh, U., 2006. Palaeo-moisture evolution in monsoonal Central Asia during the last 50,000 years. Quat. Sci. Rev. 25, 163–178.
Herzschuh, U., Zhang, C.J., Mischke, S., Herzschuh, R., Mohammadi, F., Mingram, B., Kurschner, H., Riedel, F., 2005. A late Quaternary lake record from the Qilian Mountains (NW China): evolution of the primary production and the water depth reconstructed from macrofossil, pollen, biomarker, and isotope data. Glob. Planet. Change 46, 361–379.
Herzschuh, U., Kurschner, H., Mischke, S., 2006. Temperature variability and vertical vegetation belt shifts during the last ~50,000 yr in the Qilian Mountains (NE margin of the Tibetan Plateau, China). Quat. Res. 66, 133–146.
Heyman, J., Stroeven, A.P., Caffee, M.W., Haettestrand, C., Harbor, J.M., Li, Y., Alexanderson, H., Zhou, L., Hubbard, A., 2011a. Palaeoglaciology of Bayan Har Shan, NE Tibetan Plateau; exposure ages reveal a missing LGM expansion. Quat. Sci. Rev. 30, 1988–2001.
Heyman, J., Stroeven, A.P., Harbor, J.M., Caffee, M.W., 2011b. Too young or too old: Evaluating cosmogenic exposure dating based on an analysis of compiled boulder exposure ages. Earth Planet. Sci. Lett. 302, 71–80.
Huybers, K., Roe, G.H., 2009. Spatial patterns of glaciers in response to spatial patterns in regional climate. J. Climate 22, 4606–4620.
Joshi, J.C., Ganju, A., 2010. Use of objective analysis to estimate winter temperature and precipitation at different stations over western Himalaya. J. Earth Syst. Sci. Educ. 119, 597–602.
Kim, S.J., Crowley, T.J., Erickson, D.J., Govindasamy, B., Duffy, P.B., Lee, B.Y., 2008. High-resolution climate simulation of the last glacial maximum. Clim. Dyn. 31, 1–16.
Kober, F., Afflinov, V., Ivy-Ochs, S., Kubik, P.W., Wieler, R., 2011. The cosmogenic ^{21}Ne production rate in quartz evaluated on a large set of existing ^{21}Ne–^{10}Be data. Earth Planet. Sci. Lett. 302, 163–171.
Kohl, C.P., Nishiizumi, K., 1992. Chemical isolation of quartz for measurement of in situ-produced cosmogenic nuclides. Geochim. Cosmochim. Acta 56, 3583–3587.
Kong, P., Na, C., Fink, D., Zhao, X., Xiao, W., 2009. Moraine dam related to late Quaternary glaciation in the Yulong Mountains, southwest China, and impacts on the Jinsha River. Quat. Sci. Rev. 28, 3224–3235.
Kutzbach, J.E., 1981. Monsoon climate of the early Holocene: Climate experiment with the earth's orbital parameters for 9000 years ago. Science 214, 59–61.
Lehmkuhl, F., Owen, L.A., 2005. Late Quaternary glaciation of Tibet and the bordering mountains: a review. Boreas 34, 87–100.
NGRIP Project, 2004. North Greenland ice core project oxygen isotope data, Program, N.N.P. IGBP PAGES/World Data Center for Paleoclimatology, Boulder.
Ono, Y., Irino, T., 2004. Southern migration of westerlies in the Northern Hemisphere PEP II transect during the Last Glacial Maximum. Quat. Int. 118–119, 13–22.
Owen, L.A., Gualtieri, L., Finkel, R.C., Caffee, M.W., Benn, D.I., Sharma, M.C., 2001. Cosmogenic radionuclide dating of glacial landforms in the Lahul Himalaya, northern India; defining the timing of late Quaternary glaciation. J. Quat. Sci. 16, 555–563.
Owen, L.A., Finkel, R.C., Caffee, M.W., 2002. A note on the extent of glaciation throughout the Himalaya during the global last glacial maximum. Quat. Sci. Rev. 21, 147–157.
Owen, L.A., Finkel, R.C., Barnard, P.L., Ma, H., Asahi, K., Caffee, M.W., Derbyshire, E., 2005. Climatic and topographic controls on the style and timing of late Quaternary glaciation throughout Tibet and the Himalaya defined by ^{10}Be cosmogenic radionuclide surface exposure dating. Quat. Sci. Rev. 24, 1391–1411.
Owen, L.A., Caffee, M.W., Bovard, K.R., Finkel, R.C., Sharma, M.C., 2006a. Terrestrial cosmogenic nuclide surface exposure dating of the oldest glacial successions in the Himalayan orogen: Ladakh Range, northern India. Geol. Soc. Am. Bull. 118, 383–392.
Owen, L.A., Chaolu, Y., Finkel, R.C., Davis, N.K., 2010. Quaternary glaciation of Gurla Mandhata (Naimon'anyi). Quat. Sci. Rev. 29, 1817–1830.
Owen, L.A., Chen, J., Hedrick, K.A., Caffee, M.W., Robinson, A.C., Schoenbohm, L.M., Yuan, Z., Li, W., Imrecke, D.B., Liu, J., 2012. Quaternary glaciation of the Tashkurgan Valley, Southeast Pamir. Quat. Sci. Rev. 47, 56–72.
Pratt-Sitaula, B., 2004. Glaciers, climate, and topography in the Nepalese Himalaya. PhD thesis. UC Santa Barbara, Santa Barbara.
Prell, W.L., Kutzbach, J.E., 1992. Sensitivity of the Indian Monsoon to forcing parameters and implications for its evolution. Nature 360, 647–652.
Putkonen, J., Swanson, T., 2003. Accuracy of cosmogenic ages for moraines. Quat. Res. 59, 255–261.
Putnam, A.E., Schaefer, J., Barrell, D.J.A., Vendergoes, M., Denton, G.H., Kaplan, M.R., Finkel, R.C., Schwartz, R., Goehring, B., Kelley, S.E., 2010. In situ cosmogenic ^{10}Be production-rate calibration from the Southern Alps, New Zealand. Quat. Geochronol. 5 (4), 392–409.
Richards, B.W., Owen, L.A., Rhodes, E.J., 2000a. Timing of late Quaternary glaciations in the Himalayas of northern Pakistan. J. Quat. Sci. 15, 283–297.
Richards, B.W.M., Benn, D.I., Owen, L.A., Rhodes, E.J., Spencer, J.Q., 2000b. Timing of late Quaternary glaciations south of Mount Everest in the Khumbu Himal, Nepal. Geol. Soc. Am. Bull. 112, 1621–1632.
Rodell, M., Houser, P.R., Jambor, U., Gottschalck, J., Mitchell, K., Meng, C.J., Arsenault, K., Cosgrove, B., Radakovich, J., Bosilovich, M., Entin, J.K., Walker, J.P., Lohmann, D., Toll, D., 2004. The global land data assimilation system. Bull. Am. Meteorol. Soc. 85, 381–389.
Roe, G.H., 2011. What do glaciers tell us about climate variability and climate change? J. Glaciol. 57, 567–578.
Roe, G.H., O'Neal, M.A., 2009. The response of glaciers to intrinsic climate variability: Observations and models of late-Holocene variations in the Pacific northwest. J. Glaciol. 55, 839–854.
Rood, D.H., Hall, S., Guilderson, T.P., Finkel, R.C., Brown, T.A., 2010. Challenges and opportunities in high-precision Be-10 measurements at CAMS. Nucl. Instrum. Methods Phys. Res., Sect. B, Beam Interact. Mater. Atoms 268, 730–732.
Rood, D.H., Brown, T.A., Finkel, R.C., Guilderson, T.P., 2013. Poisson and non-Poisson uncertainty estimations of ^{10}Be/^{9}Be measurements at LLNL-CAMS. Nucl. Instrum. Methods Phys. Res., Sect. B, Beam Interact. Mater. Atoms 294, 426–429.
Rupper, S., Roe, G., 2008. Glacier changes and regional climate: A mass and energy balance approach. J. Climate 21, 5384–5401.
Rupper, S., Roe, G., Gillespie, A., 2009. Spatial patterns of Holocene glacier advance and retreat in Central Asia. Quat. Res. 72, 337–346.
Schafer, J.M., Oberholzer, P., Zhao, Z., Ivy-Ochs, S., Wieler, R., Baur, H., Kubik, P.W., Schluchter, C., 2008. Cosmogenic beryllium-10 and neon-21 dating of late Pleistocene glaciations in Nyalam, monsoonal Himalayas. Quat. Sci. Rev. 27, 295–311.
Scherler, D., Bookhagen, B., Strecker, M.R., von Blanckenburg F, Rood, D., 2010. Timing and extent of late Quaternary glaciation in the western Himalaya constrained by ^{10}Be moraine dating in Garhwal, India. Quat. Sci. Rev. 29, 815–831.
Seong, Y.B., Owen, L.A., Bishop, M.P., Bush, A., Clendon, P., Copland, L., Finkel, R.C., Kamp, U., Shroder Jr., J.F., 2007. Quaternary glacial history of the central Karakoram. Quat. Sci. Rev. 26, 3384–3405.
Shackleton, N.J., 2000. The 100,000-year ice-age cycle identified and found to lag temperature, carbon dioxide, and orbital eccentricity. Science 289, 1897–1902.
Shi, Y., 2002. Characteristics of late Quaternary monsoonal glaciation on the Tibetan Plateau and in East Asia. Quat. Int. 97–98, 79–91.
Shi, Y., Yu, G., Liu, X., Li, B., Yao, T., 2001. Reconstruction of the 30–40 ka BP enhanced Indian monsoon climate based on geological records from the Tibetan Plateau. Palaeogeogr. Palaeoclimatol. Palaeoecol. 169, 69–83.
Shin, S., Liu, L., Otto-Bliesner, O.-B., Brady, B., Kutzbach, K., Harrison, H., 2003. A simulation of the last glacial maximum climate using the NCAR-CCSM. Clim. Dyn. 20, 127–151.
Sternai, P., Herman, F., Fox, M.R., Castelltort, S., 2011. Hypsometric analysis to identify spatially variable glacial erosion. J. Geophys. Res. 116, F03001, http://dx.doi.org/10.1029/2010JF001823.
Strasky, S., Graf, A.A., Zhao, Z., Kubik, P.W., Baur, H., Schlüchter, C., Wieler, R., 2009. Late-glacial ice advances in southeast Tibet. J. Asian Earth Sci. 34, 458–465.
Strobl, M., Hetzel, R., Niedermann, S., Ding, L., Zhang, L., 2012. Landscape evolution of a bedrock peneplain on the southern Tibetan Plateau revealed by in situ-produced cosmogenic ^{10}Be and ^{21}Ne. Geomorphology 153–154, 192–204.
Taylor, P.J., Mitchell, W.A., 2000. The Quaternary glacial history of the Zanskar Range, north–west Indian Himalaya. Quat. Int. 65–66, 81–99.
Thompson, L.G., Yao, T., Davis, M.E., Henderson, K.A., Mosley-Thompson, E., Lin, P.N., Beer, J., Synal, H.A., Cole-Dai, J., Bolzan, J.F., 1997. Tropical climate instability: The last glacial cycle from a Qinghai–Tibetan ice core. Science 276, 1821–1825.
Tsukamoto, S., Asahi, K., Watanabe, T., Rink, W.J., 2002. Timing of past glaciations in Kanchenjunga Himal, Nepal by optically stimulated luminescence dating of tills. Quat. Int. 97–98, 57–67.
Wang, Y.J., Cheng, H., Edwards, R.L., Kong, X.G., Shao, X.H., Chen, S.T., Wu, J.Y., Jiang, X.Y., Wang, X.F., An, Z.S., 2008. Millennial- and orbital-scale changes in the East Asian monsoon over the past 224,000 years. Nature 451, 1090–1093.

Wünnemann, B., Demske, D., Tarasov, P., Kotlia, B.S., Reinhardt, C., Bloemendal, J., Diekmann, B., Hartmann, K., Krois, J., Riedel, F., Arya, N., 2010. Hydrological evolution during the last 15 kyr in the Tso Kar lake basin (Ladakh, India), derived from geomorphological, sedimentological and palynological records. Quat. Sci. Rev. 29, 1138–1155.

Yadav, R.K., 2009. Role of equatorial central Pacific and northwest of North Atlantic 2-metre surface temperatures in modulating Indian summer monsoon variability. Clim. Dyn. 32, 549–563.

Yadav, D.N., Chauhan, M.S., Sarin, M.M., 2006. Geochemical and pollen proxy records from northeastern Madhya Pradesh: An appraisal of late-Quaternary vegetation and climate change. J. Geol. Soc. India 68, 95–102.

Yao, T., Jiao, J., Zhang, X., 1992. Glacial study on the Guliya Ice Cap. J. Glaciol. Geocryol. 14, 233–241.

Yatagai, A., Kamiguchi, K., Arakawa, O., Hamada, A., Yasutomi, N., Kitoh, A., 2012. APHRODITE: Constructing a Long-term Daily Gridded Precipitation Dataset for Asia based on a Dense Network of Rain Gauges. Bull. Am. Meteorol. Soc. 93, 1401–1415.

Zech, R., Glaser, B., Sosin, P., Kubik, P.W., Zech, W., 2005b. Evidence for long-lasting landform surface instability on hummocky moraines in the Pamir Mountains (Tajikistan) from (super 10)Be surface exposure dating. Earth Planet. Sci. Lett. 237, 453–461.

Zhang, Y., Liu, S., Ding, Y., 2006. Observed degree-day factors and their spatial variation on glaciers in western China. Ann. Glaciol. 43, 301–306.

Zhang, Z., Gong, D., Hu, M., Guo, D., He, X., Lei, Y., 2009. Anomalous winter temperature and precipitation events in southern China. J. Geogr. Sci. 19, 471–488.

Further reading

Abramowski, U., Bergau, A., Seebach, D., Zech, R., Glaser, B., Sosin, P., Kubik, P.W., Zech, W., 2006. Pleistocene glaciations of Central Asia; results from ^{10}Be surface exposure ages of erratic boulders from the Pamir (Tajikistan), and the Alay–Turkestan Range (Kyrgyzstan). Quat. Sci. Rev. 25, 1080–1096.

Barnard, P.L., Owen, L.A., Finkel, R.C., 2004a. Style and timing of glacial and paraglacial sedimentation in a monsoon-influenced high Himalayan environment, the upper Bhagirathi Valley, Garhwal Himalaya. Sediment. Geol. 165, 199–221.

Barnard, P.L., Owen, L.A., Sharma, M.C., Finkel, R.C., 2004b. Late Quaternary (Holocene) landscape evolution of a monsoon-influenced high Himalayan valley, Gori Ganga, Nanda Devi, NE Garhwal. Geomorphology 61, 91–110.

Dortch, J.M., Owen, L.A., Caffee, M.W., 2010. Quaternary glaciation in the Nubra and Shyok valley confluence, northernmost Ladakh, India. Quat. Res. 74, 132–144.

Lasserre, C., Gaudemer, Y., Tapponnier, P., Meriaux, A.S., van der Woerd, J., Ryerson, F.J., Finkel, R.C., Caffee, M.W., 2002. Fast late Pleistocene slip rate on the Leng Long Ling Segment of the Haiyuan Fault, Qinghai, China. J. Geophys. Res. 107, 15.

Meriaux, A.S., Ryerson, F.J., Tapponnier, P., van der Woerd, J., Finkel, R.C., Xu, X.c., Xu, Z.d., Caffee, M.W., 2004. Rapid slip along the central Altyn Tagh Fault; morphochronologic evidence from Cherchen He and Sulamu Tagh. J. Geophys. Res. 109, 23.

Nishiizumi, K., Imamura, M., Caffee, M., Southon, J.R., Finkel, R.C., McAninch, J., 2007. Absolute calibration of ^{10}Be AMS standards. Nucl. Instrum. Methods Phys. Res. B258, 403–413.

Owen, L.A., Derbyshire, E., Spencer, J.Q., Barnard, P.L., Finkel, R.C., Caffee, M.W., 2003a. The timing and style of late Quaternary glaciation in the La Ji Mountains, NE Tibet; evidence for restricted glaciation during the latter part of the last glacial. Zeitschrift fuer Geomorphologie. Supplementband, vol. 130. Gebrueder Borntraeger, Federal Republic of Germany (DEU), Berlin–Stuttgart, pp. 263–276.

Owen, L.A., Finkel, R.C., Haizhou, M., Spencer, J.Q., Derbyshire, E., Barnard, P.L., Caffee, M.W., 2003b. Timing and style of Late Quaternary glaciation in northeastern Tibet. Geol. Soc. Am. Bull. 115, 1356–1364.

Owen, L.A., Finkel, R.C., Haizhou, M., Barnard, P.L., 2006b. Late Quaternary landscape evolution in the Kunlun Mountains and Qaidam Basin, Northern Tibet: A framework for examining the links between glaciation, lake level changes and alluvial fan formation. Quat. Int. 154, 73–86.

Owen, L.A., Robinson, R., Benn, D.I., Finkel, R.C., Davis, N.K., Yi, C., Putkonen, J., Li, D., Murray, A.S., 2009. Quaternary glaciation of Mount Everest. Quat. Sci. Rev. 28, 1412–1433.

Phillips, W.M., Sloan, V.F., Shroder, J.F., Sharma, P., Clarke, M.L., Rendell, H.M., 2000. Asynchronous glaciation at Nanga Parbat, northwestern Himalaya Mountains, Pakistan. Geology 28, 431–434.

Schafer, J.M., Tschudi, S., Zhao, Z., Wu, X., Ivy-Ochs, S., Wieler, R., Baur, H., Kubik, P.W., Schluchter, C., 2002. The limited influence of glaciations in Tibet on global climate over the past 170 000 yr. Earth Planet. Sci. Lett. 194, 287–297.

Seong, Y.B., Owen, L.A., Yi, C.L., Finkel, R.C., 2009. Quaternary glaciation of Muztag Ata and Kongur Shan: Evidence for glacier response to rapid climate changes throughout the Late Glacial and Holocene in westernmost Tibet. Geol. Soc. Am. Bull. 121, 348–365.

Zech, R., Abramowski, U., Glaser, B., Sosin, P., Kubik, P.W., Zech, W., 2005a. Late Quaternary glacial and climate history of the Pamir Mountains derived from cosmogenic ^{10}Be exposure ages. Quat. Res. 64, 212–220.